Petroleum Science 21 (2024) 667–673

Contents lists available at ScienceDirect

Petroleum Science

journal homepage: www.keaipublishing.com/en/journals/petroleum-science

Original Paper

Adhesion strength of tetrahydrofuran hydrates is dictated by substrate stiffness

Yan-Wen Lin [a, b], Tong Li [b, c, *], Yi Zhang [b], Wei-Wei Yan [b], Xiao-Ming Chen [d, e, **], Zhi-Sen Zhang [a], Jian-Yang Wu [a, f]

[a] Department of Physics, Research Institute for Biomimetics and Soft Matter, Jiujiang Research Institute and Fujian Provincial Key Laboratory for Soft Functional Materials Research, Xiamen University, Xiamen, 361005, Fujian, China
[b] Key Laboratory of Marine Materials and Related Technologies, Zhejiang Key Laboratory of Marine Materials and Protective Technologies, Ningbo Institute of Materials Technology and Engineering, Chinese Academy of Sciences, Ningbo, 315201, Zhejiang, China
[c] Key Laboratory of Icing and Anti/De-icing, China Aerodynamics Research and Development Center, Mianyang, 621000, Sichuan, China
[d] Micro- and Nano-technology Research Center, State Key Laboratory for Manufacturing Systems Engineering, Xi'an Jiaotong University, Xi'an, 710049, Shaanxi, China
[e] Electronic Materials Research Lab, Key Laboratory of the Ministry of Education, Xi'an Jiaotong University, Xi'an, 710049, Shaanxi, China
[f] NTNU Nanomechanical Lab, Norwegian University of Science and Technology (NTNU), Trondheim, 7491, Norway

ARTICLE INFO

Article history:
Received 18 December 2022
Received in revised form
16 March 2023
Accepted 8 August 2023
Available online 9 August 2023

Edited by Jia-Jia Fei and Min Li

Keywords:
Hydrate
Adhesion strength
Elastic modulus
Coatings

ABSTRACT

Understanding the hydrate adhesion is important to tackling hydrate accretion in petro-pipelines. Herein, the relationship between the Tetrahydrofuran (THF) hydrate adhesion strength (AS) and surface stiffness on elastic coatings is systemically examined by experimental shear force measurements and theoretical methods. The mechanical factor-elastic modulus of the coatings greatly dictates the hydrate AS, which is explained by the adhesion mechanics theory, beyond the usual factors such as wettability and structural roughness. Moreover, the hydrate AS increases with reducing the thickness of the elastic coatings, resulted from the decrease of the apparent surface elastic modulus. The effect of critical thickness for the elastic materials with variable elastic modulus on the hydrate AS is also revealed. This study provides deep perspectives on the regulation of the hydrate AS by the elastic modulus of elastic materials, which is of significance to design anti-hydrate surfaces for mitigation of hydrate accretion in petro-pipelines.

1. Introduction

Clathrate hydrates are ice-like crystalline solids, in which water molecules are uniquely arranged to form polyhedral cages that are able to entrap diverse small molecules such as methane, carbon dioxide, tetrahydrofuran (THF), and so forth (Fang et al., 2019; Nahri et al., 2019; Wu et al., 2015, 2017; Xu et al., 2020). As one of the most promising energy sources, natural gas hydrates (NGHs) possess a high capacity to store natural gas, which is increasingly recognized as an alternative fuel resource, thereby they attracted much attention (Lin et al., 2022a, b; Pang et al., 2021; Wang et al., 2022b; Xu et al., 2022a, b; Yang et al., 2023). NGHs commonly occur in the seafloor and subterranean permafrost sediments under harsh conditions including high pressure and low temperature as well as in oil and gas pipelines. However, the accretion of clathrate hydrates on the inner surface of pipelines blocks gas and oil transportation, resulting in serious safety risks and enormous economic losses (Li et al., 2016; Ning et al., 2012; Zhang et al., 2020).

To date, a number of approaches including insulation, dehydration, heating and inhibition with chemicals have been implemented to handle the hydrate formation in the pipelines to reduce the safety hazards (Li et al., 2016; Zhang et al., 2020). Those approaches, however, are commonly regarded as active methods. To prevent the formation of hydrate inside the gas and oil pipelines, the method of heating pipes (Zhang et al., 2018), adding alcohols such as methanol (Wang et al., 2019) to shift the thermodynamic equilibrium away from the hydrate formation, while the utilization

* Corresponding author.
** Corresponding author.
E-mail addresses: tong@nimte.ac.cn (T. Li), xiaomingchen@xjtu.edu.cn (X.-M. Chen).

https://doi.org/10.1016/j.petsci.2023.08.009

of kinetic inhibitors is to retard hydrate crystallization and growth (Charlton et al., 2018; Hu et al., 2019). However, those active methods to mitigate hydrate plugging in gas and oil pipelines are usually costly, energy-consuming, and may bring about detrimental environmental problems (Sloan, 2003; Smith et al., 2012; Sum et al., 2009). To alleviate the issue of hydrate blockage in oil and gas pipelines, it is crucial to have a good understanding of factors that affect the hydrate adhesion strength (AS) on solid surfaces and develop eco-friendly, low-cost, and efficient way anti-hydrate approaches.

Substantive interests have been focused on the development of passive hydrate-phobic coatings on the petro-pipelines. Those coatings can inhibit hydrate formation and/or reduce hydrate AS on the petro-pipelines, allowing for hydrate removal without the external force or energy (Fan et al., 2020; Ma et al., 2021; Ragunathan et al., 2019; Smith et al., 2012; Sojoudi et al., 2018; Zhang et al., 2021). On the basis of these studies, many external factors influencing the hydrate AS were summarized (Liu et al., 2020a, b, 2022). For example, the cyclopentane (CyC5) hydrate deposits AS decreases dramatically with the concentration of hydrate inhibitors such as ethylene glycol or glycerol (Liu et al., 2022). The coproduced solids including sand, scale and wax as well as surface corrosion affect the sintered hydrate deposit AS (Liu et al., 2020b). In additions, the effects of the subcooling, formation time, roughness of surface and material types on the hydrate AS were revealed, indicating that hydrate AS is determined by many external factors (Liu et al., 2020a). Recently, the anti-hydrate surfaces were designed by learning from the design concepts of anti-icing coatings (Dou et al., 2014; Li et al., 2019, 2020, 2022; Wang et al., 2022a) on the basis of the adhesion mechanics proposed by Griffith and further elaborated by Kendall (1971). According to this adhesion mechanics theory, the critical shear stress required to separate a rigid object (e.g., ice) from a film is as follows:

$$\tau \propto \sqrt{\frac{W\mu}{t}}$$

where W, μ and t are the work of adhesion between ice and the surface, the shear modulus, and the thickness of the coating. For isotropic materials, it is estimated that the shear modulus is $\mu = E/3$, where E is Young's modulus (Ibanez-Ibanez et al., 2022; Wang et al., 2014). It is revealed that the ice AS is tuned by tailoring the chemical and physical characteristics of the substrate that the ice adheres to. Recently, the design concept of reducing hydrate AS using hydrophobicity through controlling surface factors including chemical composition and surface structure has been widely accepted, emerging the approaches such as the super-hydrophobic, slippery surface for hydrate-phobicity (Aman et al., 2014; Fan et al., 2020; Sojoudi et al., 2015). So far, these surfaces are still faced with poor durability and mechanical weakness, restricting them from practical application. The effects of materials' mechanical factors such as stiffness on the hydrate AS remain unexplored, although there have been several reports on the ice AS (Ibanez-Ibanez et al., 2022; Regulagadda et al., 2022). For example, the sandwich-like PDMS was manufactured by a facile low-cost preparation method for lowering the ice AS, showing that elastic modulus of elastomer coating is controllable by adjusting the weight ratio of the PDMS base-to-curing agent (Beemer et al., 2016). The effect of the elastic modulus of elastomeric coating on ice AS were experimentally investigated (Wang et al., 2014), providing the generalized concept for the removal of ice from low modulus elastomers. On the basic of the principles of adhesion mechanics, the effect of shear modulus on ice AS was investigated, and the inexpensive, non-corrosive PDMS gels with outstanding mechanical durability are developed and applied to prevent icing (Beemer et al., 2016). Whereas for the hydrate accretion issue, there is an urgent need to develop the surface based on the regulation of elastic modulus that possesses low hydrate AS for practical applications in gas and oil pipelines. However, the question is raised as to whether the design concept of the anti-icing coating by mechanical factors can be borrowed for the hydrate low-adhesion coating is still pending.

In this work, THF hydrate/ice directly forms on polydimethysiloxane (PDMS) coatings at temperature of −20 °C for examining the THF hydrate/ice AS. The THF hydrate/ice AS on the PDMS coatings under shear load is investigated by experimental shear force measurements and theoretical method. The effect of the elastic modulus of PDMS coatings on THF hydrate AS are comprehensively explored. In addition, the effect of thickness of materials with variable elastic modulus on the hydrate AS is revealed, indicating a clear relationship between hydrate AS and deformation caused by coating thickness and elastic modulus. This work provides insights and perspective to the understanding of hydrate AS, which is of great help to clear the blockage by hydrate accretion in the gas and oil pipelines.

2. Experimental

2.1. Materials and chemicals

Tetrahydrofuran (THF, ≥99.9%), ethanol (99.7%) and acetone (99.5%) were supplied by Sinopharm Chemical Reagent Co., Ltd. (Shanghai, China). PDMS (Sylgard 184) precursor was bought from Dow Corning Co. Ltd. (USA). All chemicals were used as received without any further purification. Glass slides were purchased from Taobao Ltd. Deionized (DI) water with a resistivity higher than 15 MΩ cm was used in all experiments.

2.2. Methods

2.2.1. Shear adhesion strength test

The ice/THF hydrate AS on PDMS coatings was measured by a homemade shear adhesion testing apparatus consisting of a linear stage (X-LRT0100AL-E08C), force gauge (ZTS-500N) with force sensor and cooling stage, as shown in Fig. 1. A polypropylene tube with 15.0 mm inner diameter is placed on the rigid glass slide with PDMS coatings in the refrigerator with −20 °C. Then, circa (ca.) 2 mL DI water/19 wt% THF solution is injected into the polypropylene tube. The preparation of 19 wt% THF solution can be referred to Supporting Information. The samples frozen in the refrigerator at −20 °C for more than 4 h to ensure complete freezing. Before adhesion testing, the frozen samples with PDMS coatings are moved to the cooling stage at −20 °C. Next, the probe of the force sensor at a constant velocity of 0.075 mm/s is propelled into the THF hydrate/ice tube for obtaining the force required to

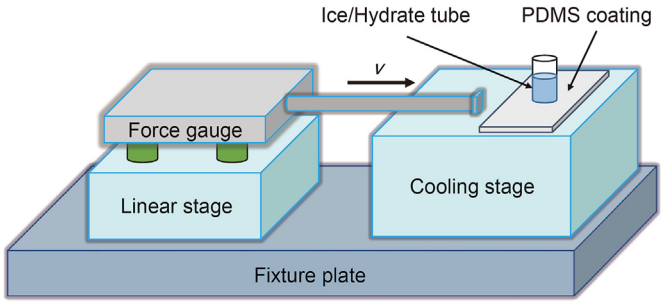

Fig. 1. Schematic depiction of the shear adhesion equipment consisting of a linear stage, force gauge and cooling stage.

detach each ice/THF hydrate. The probe velocity was controlled by using an electric displacement stage. The force required to detach each ice/THF hydrate tube from the PDMS coating was obtained. The probe was located ca.1.0 mm above the PDMS coating to minimize torque on the ice/THF hydrate sample. This distance remained the same for all samples. The force measurement tests are performed at least 3 times for each sample to improve accuracy. The measured maximum fracture forces were converted into ice/THF hydrate AS by dividing over the known cross-sectional area (1.766 cm^2) of the ice-/THF hydrate-PDMS coating interface.

2.2.2. Finite element (FE) simulations

To reveal the interfacial adhesion properties between hydrate and elastomer coatings, the FE models are established by using the commercial software ABAQUS to simulate the shear process, as shown in Fig. 2. The Young's Modulus of hydrate is set to be 600 MPa. In order to reveal the effect of the elastic modulus of the PDMS coating on the hydrate AS, elastic modulus of 1.0, 1.5 and 2.0 MPa for the FE models are considered. The bottom of PDMS coatings are fixed in all six degrees of freedom. As for the hydrate, the velocity applied in the bottom area of the hydrate tube in x direction is set to be 0.075 mm/s, whereas zero velocity is assigned in the other two (y and z) directions, as indicated in Fig. 2(a). The interfacial interaction between hydrates and PDMS coatings is described by the cohesive elements. The tetrahedron element with 4 vertices, 6 edges, and bounded by 4 triangular faces have been adopted for FE simulation because the tetrahedron elements possess the advantages of simple geometric features and strong description ability. As illustrated in Fig. 2(b), the parts were meshed with tetrahedron elements using the FE mesh generator.

3. Results and discussions

3.1. Design and characterization of PDMS coatings

To examine the effects of the mechanical factor: stiffness on hydrate AS, the Sylgard 184 is used to prepare silicone-based PDMS coatings with varied elastic modulus by various weight ratios of PDMS base-to-curing agent. The PDMS base and curing agent with the weight ratio of 2:1, 5:1, 10:1, 20:1 and 30:1 were thoroughly mixed, in which the preparation process of PDMS coatings is illustrated in Fig. 3(a). Details of the preparation of PDMS coatings and their characterization can be referred to in Supporting Information. Fig. 3(b) shows the three-dimensional (3D) AFM images of PDMS coatings composed of different weight ratios of PDMS base-to-curing agent, in which the surface of 2:1 coating shows a rougher morphology than other coatings. As is depicted in Fig. 3(c), the root mean square (RMS) roughness of the 5:1–30:1 PDMS coatings are lower than 5 nm and ranges in a quite low state, with an estimation area of 5 μm × 5 μm from the AFM images. For PDMS coating prepared with 2:1 wt ratio of PDMS base-to-curing agent, large content of curing agent causes a liquid layer on the surface of the coating (Golovin et al., 2016; Ibanez-Ibanez et al., 2022), thereby observing a rougher surface than other samples because the AFM probe may be largely deformed due to the interactions between AFM probe and the liquid layer. For the other coatings, the contact angles (CA) of water droplets on those PDMS coatings is almost unchanged varying from 104° to 114° with the increase of PDMS-base content. Moreover, the small difference between the advancing/receding CA (see Fig. S1) of water droplets of the 5:1–30:1 coatings indicates that the surface energy plays a similar role in the hydrate AS. Fig. 3(d) shows the elastic modulus of as-obtained PDMS coatings as a function of the weight ratio of PDMS base-to-curing agent. Intriguingly, there is "flipped behavior" in the elastic modulus of PDMS coatings; the elastic modulus initially increases, but then decreases with increasing the content of PDMS base, with the maximum elastic modulus of around 1.80 MPa at the weight ratio of PDMS base-to-curing agent of 10:1. In addition, the 10:1 and 2:1 coatings show the highest tensile strength and the largest friction coefficient, respectively (see Table S1).

3.2. Hydrate adhesion strength on PDMS coatings with variable elastic modulus

Fig. 4(a) illustrates the schematic diagram for the measurement of the AS, in which the probe of the force sensor into the ice/THF hydrate tube is parallel to the ice-/hydrate-surface interface. Then, a shear speed of 0.075 mm/s is imposed to propel the probe of the force sensor into one side of the ice/THF hydrate tube. The peak force required to break the ice-/hydrate-surface interface is recorded. Here, the average AS of ice-/hydrate-surface interface is defined by dividing the peak force by the cross-sectional area of ice/hydrate. It should be noted that each sample is tested at least 3 times to improve accuracy. Fig. 4(b) shows the ice/THF hydrate AS on the coatings as a function of the weight ratio of the PDMS base-to-curing agent, as well as the ratio of the AS of ice-to-THF hydrate. Apparently, the THF hydrate/ice on the PDMS coatings with variable elastic modulus show different ASs (below 100 × 10^3 Pa) as they are subjected to a shear load. Interestingly, there is also "flipped behavior" in both ice and THF hydrate AS; with increasing the content of PDMS base, the ice/THF hydrate AS initially increases and then declines. The THF hydrate/ice AS increases from around 25.70/18.68 kPa to 75.42/62.46 kPa as the weight ratio of PDMS base-to-curing agent varies from 2:1 to 10:1, but then decreases from around 75.42/62.46 kPa to 37.70/26.98 kPa with the weight ratio varying from 10:1 to 30:1. In addition, the AS of ice on the 2:1 coating with the surface liquid phase is around 1.35 times than that of the THF hydrate. Whereas for other samples, it is observed that the ratio of ice-to-THF hydrate AS varies from about 1.30 to 1.56, depending on the elastic modulus of PDMS coating.

To reveal the role of the mechanical factor: stiffness on the shear

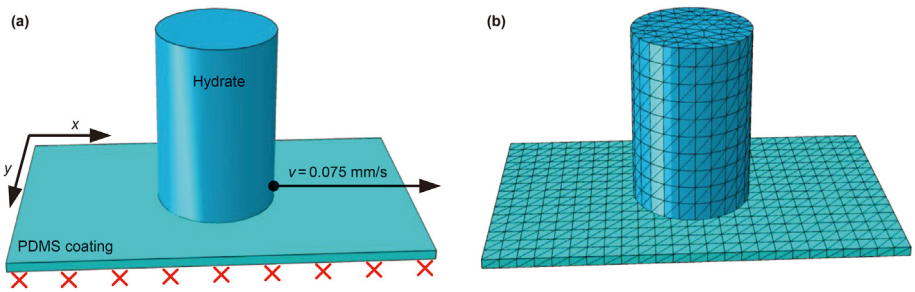

Fig. 2. Hydrate-PDMS coating is modeled using FE method. (**a**) Boundary conditions of FE model, the bottom of PDMS coating were fixed. (**b**) The meshed FE model.

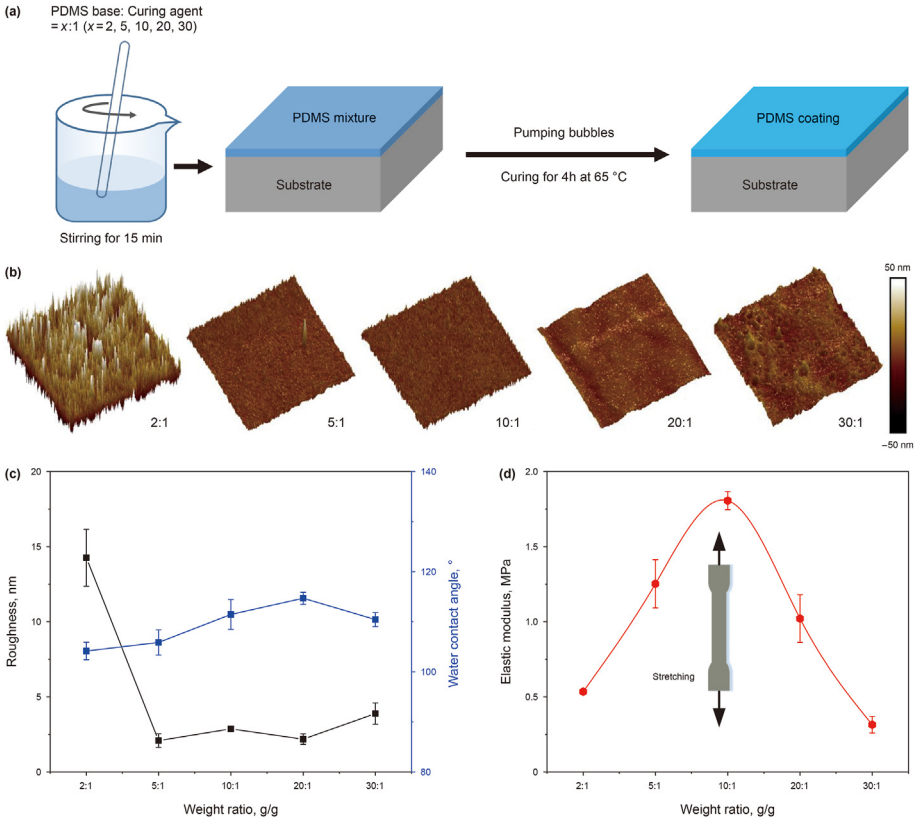

Fig. 3. Schematic of the preparation and characterization of PDMS coatings. (**a**) Schematic diagram of the preparation process of PDMS coatings with various weight ratios of PDMS base-to-curing agent. (**b**) AFM morphologies of PDMS coatings with different weight ratios of PDMS base-to-curing agent. (**c**) The roughness and water CA and (**d**) elastic modulus of PDMS coatings as a function of the weight ratio of PDMS base-to-curing agent.

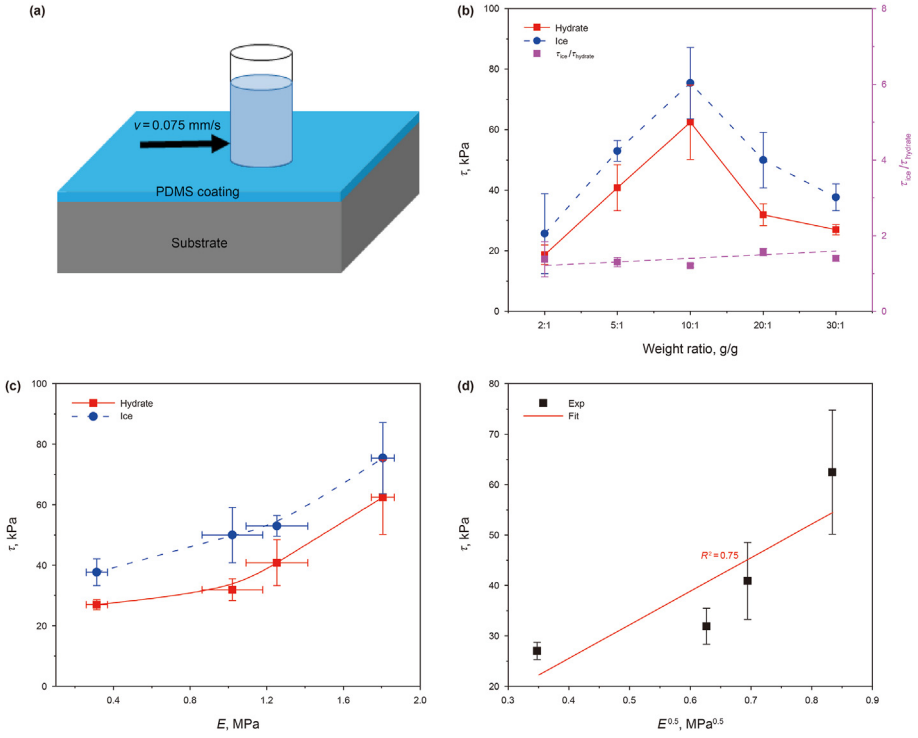

Fig. 4. The AS of ice/THF hydrate on PDMS coatings prepared with varied weight ratios of PDMS base-to-curing agent. (**a**) Schematic diagram of ice/THF hydrate shear adhesion tester. (**b**) The AS of ice/THF hydrate on PDMS coatings as a function of the weight ratio of PDMS base-to-curing agent. (**c**) Ice/THF hydrate AS as a function of the elastic modulus of PDMS coatings. (**d**) The shear AS of THF hydrate is proportional to the 0.5th power of elastic modulus. Each sample is tested at least 3 times to improve the accuracy.

AS, the abovementioned interfacial adhesion mechanics theory are employed for analysis. Fig. 4(c) shows the ice/THF hydrate AS as a function of the elastic modulus of the PDMS coatings. As is shown, the ice/hydrate AS increases with the elastic modulus, revealing the positive correlation of ice/hydrate AS with the elastic modulus. This is indicative of the substrate stiffness that dictates the ice/hydrate AS. As the THF hydrate is sheared on the PDMS coatings, the elastomer coating is locally stretched and the elastic stretching increases the elastic potential energy, thereby generating the maximum shear force (Kim et al., 2007). When a shear force is imposed, stress accumulation is concentrated in the vicinity of the ice/hydrate-substrate interface, thereby promoting ice/hydrate detachment from the coatings (Wang et al., 2014; Yeong et al., 2016, 2018). Furthermore, the FE simulation results also indicate that the hydrate AS increases with increasing of elastic modulus of PDMS coatings, which is consistent with our experimental results, as shown in Fig. S2. However, the hydrate AS predicted by FE simulation is slightly lower than that measured by shear adhesion tests due to the semi-empirical elastic constitutive model. The reason why the hydrate AS decreases greatly with the low elastic modulus is explained as follows: the PDMS coating with low elastic modulus produces a large stiffness mismatch between ice/hydrate and substrate; as a result, cracks occur more easily at the interface, thus exhibiting small AS. As is shown in Fig. 4(d), the shear AS can be successfully predicted by a single line when they are plotted as a function of $E^{0.5}$, in which the value of R^2 was 0.75, indicating that the adhesion failure of hydrate is described by the abovementioned adhesion mechanics theory. However, the deviation of the fitting curve is relatively large, which can be explained as follows. First, the Young's modulus of PDMS composed of different weight ratios of base-to-curing agent were obtained by uniaxial tensile tests, in which PDMS-based polymers are bulk materials. On the basis of the adhesion mechanics theory, interfacial AS is greatly dictated by the shear modulus and the thickness of soft materials, with relationship as $\tau \propto \sqrt{\frac{W\mu}{t}}$. In our work, it is estimated that the shear modulus is $\mu = E/3$, where E is Young's modulus (Ibanez-Ibanez et al., 2022; Wang et al., 2014). In our study, the shear modulus is obtained according to this theoretical formula. Therefore, there is difference between the shear modulus of PDMS coating and that of PDMS bulk material obtained by stretching tests. In reality, during the shear adhesion tests, however, the hydrate AS depends on the modulus of PDMS coating that is thickness dependent. Nonetheless, the fitting curve does not hinder us to reveal the changing trend of hydrate AS with $E^{0.5}$. As is indicated, the elastic modulus of the coatings is considered one of the main factors that dictate the ice/THF hydrate AS on those PDMS coatings, beyond the usual thinking that the chemical and structural factors such as wettability and surface structures dominate the hydrate AS.

3.3. Hydrate adhesion strength on PDMS coatings with different thicknesses

Herein, the effect of the thickness of the PDMS coatings on the THF hydrate AS is investigated. The shear AS measurements of hydrate are performed for the sample of the 10:1, 20:1 and 30:1 coating with different thicknesses subjected to a constant shear rate of 0.075 mm/s, respectively. Fig. 5 shows the variation of hydrate AS with the thickness of the 10:1, 20:1 and 30:1 PDMS coatings, in which the hydrate AS decreases with the increase of thickness of PDMS coatings. For the 10:1 coating, THF hydrate AS initially decreases with the increase of the PDMS coating thickness but then tends to be constant. In particular, a sudden rapid increase in THF hydrate AS is observed when the thickness of PDMS coatings is below ca. 195 μm, which is defined as the critical thickness t_0 at this value of elastic modulus. Note that the t_0 is defined as the intersection of two lines, one is of the curve at the thickness of ca. 50 μm, and the other is the tangent line of the curve at the thickness of 2000 μm. When the thickness of PDMS coatings is over ca. 195 μm, the THF hydrate AS slightly reduces. As for the 20:1 and 30:1 PDMS coatings, similar tendencies like the curve of 10:1 coating are observed in Fig. 5(a)–(c), in which the t_0 for hydrate AS increase to 418 and 517 μm, respectively. On the basic of the interfacial adhesion theoretical formula, i.e., $\tau \propto \sqrt{\frac{W\mu}{t}}$, the fitting curves between hydrate AS and $(1/t)^{1/2}$ can more clearly reveal the dependence between them. Therefore, Fig. 5(d)–(f) showed a linear relationship between THF hydrate AS and $(1/t)^{1/2}$ for these three types of PDMS coatings with different elastic moduli, in good agreement with the adhesion mechanics theory (Beemer et al., 2016; Kim et al., 2007; Wang et al., 2014). As is observed, the fitting curves based on AS and $(1/t)^{1/2}$ for 20:1 coatings demonstrate superior accuracy in predicting the changing trend of hydrate AS, where their values of R^2 are calculated to be 0.93, 0.97 and 0.92 for the 10:1, 20:1 and 30:1 PDMS coatings, respectively.

On the basis of the above experimental results, the reason for the thicker coating with lower hydrate AS is analyzed. Fig. 6(a) shows apparent elastic modulus varies with the different thicknesses of 10:1 PDMS coatings by nanoindentation tests. It is observed that the apparent elastic modulus decrease with the increase of PDMS coating thickness, which reflects the deformation ability of elastic coatings on rigid glass substrates. Therefore, the effect of thicknesses on the hydrate AS is mainly attributed to the apparent elastic modulus, which is related to the stiffness mismatch at the interface. The variation of the t_0 for hydrate AS to varied elastic modulus is discussed, as shown in Fig. 6(b). As is observed, the t_0 for hydrate AS increases with the decrease of elastics modulus for the 10:1, 20:1 and 30:1 PDMS coatings, corresponding to an increase of the t_0 from 195 to 517 μm. In addition, the map between the critical thickness, elastic modulus and hydrate AS was established, as shown in Fig. S3. It is shown that the hydrate AS on higher elastic modulus sample is more sensitive by the thickness. For the different coatings (variable elastic modulus) with the same thickness, they show varied deformational abilities due to the different elastic moduli. Notably, the stiff glass substrate restricts the deformation of PDMS coatings during the shear detachment, thereby observing lower THF hydrate AS on thicker coatings.

4. Conclusions

In summary, PDMS coatings with different elastic moduli are synthesized and expected to be utilized to prevent hydrate accretion in petro-pipelines. The mechanical factor: stiffness of PDMS coatings on the THF hydrate adhesion strength is systemically investigated by experimental shear force measurements and FE simulation.

It is shown that THF hydrate AS is greatly dictated by the elastic modulus and the thickness of the PDMS coatings. The hydrate AS increases with increasing the elastic modulus but decreases with increasing the PDMS coating thickness, originating from the decrease of the apparent elastic modulus.

The critical thickness for THF hydrate AS increases with the decrease of elastic modulus for the 10:1, 20:1 and 30:1 PDMS coatings, which corresponds to an increase of critical thickness from 195 to 517 μm for the 10:1 and 30:1 PDMS coatings, respectively. This work provides an alternative to reducing the hydrate AS by regulating the elastic modulus and thickness of solid coatings.

Declaration of competing interest

The authors declare no competing interest.

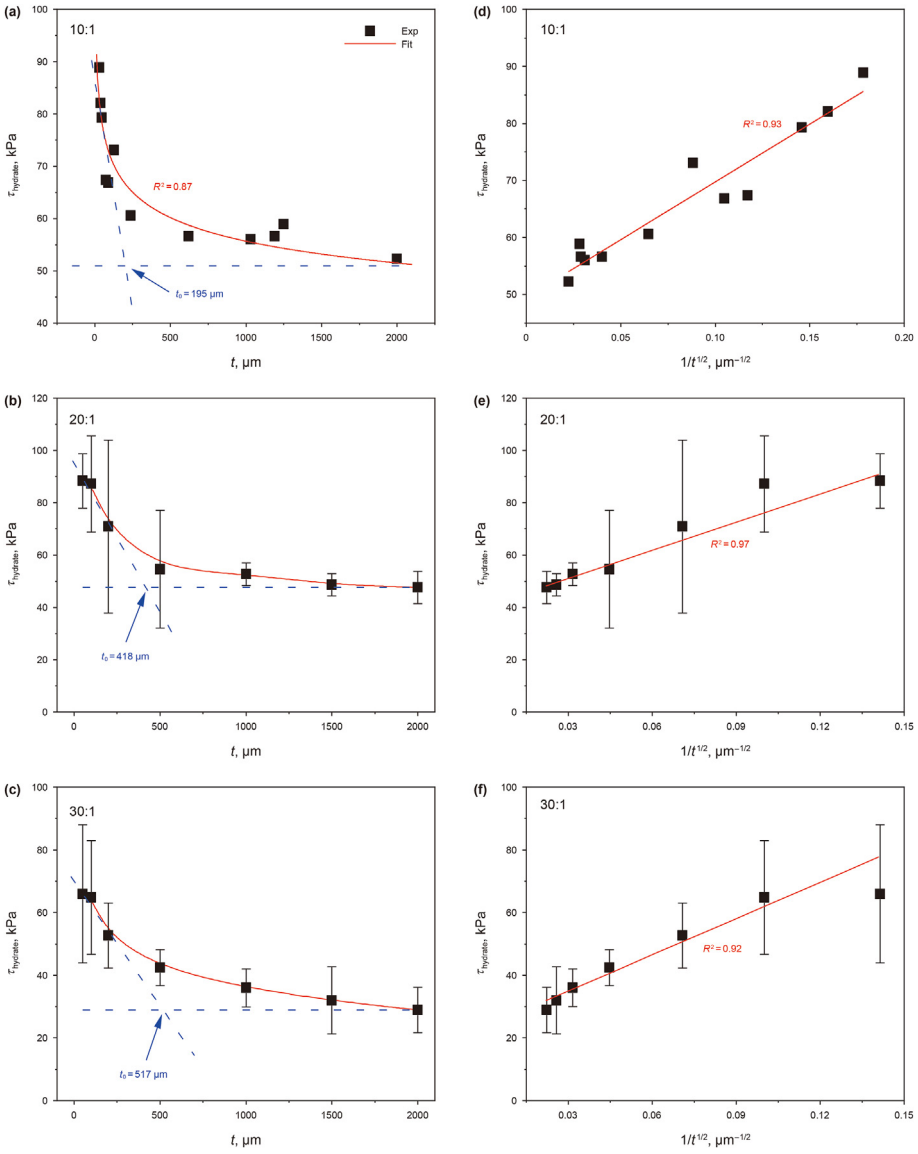

Fig. 5. The THF hydrate AS on the (**a**) 10:1, (**b**) 20:1 and (**c**) 30:1 PDMS coating as a function of the thickness of the PDMS coatings. The THF hydrate AS decreases rapidly with the thickness but then reaches a plateau for these three types of PDMS coating. The THF hydrate AS linearly increases with $(1/t)^{1/2}$ on the (**d**) 10:1, (**e**) 20:1 and (**f**) 30:1 PDMS coatings.

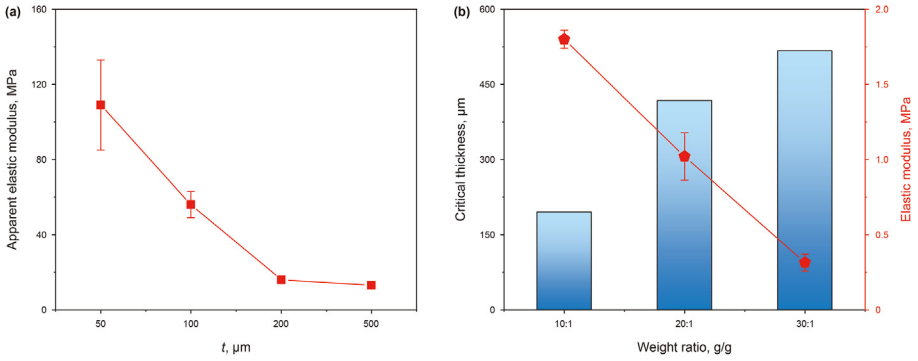

Fig. 6. (**a**) The apparent elastic modulus decreases with the increase of the thickness for the 10:1 PDMS coating. (**b**) The changing trend of the t_0 for the 10:1, 20:1 and 30:1 PDMS coatings.

Acknowledgments

This work is financially supported by the Key Laboratory of Icing and Anti/De-icing of CARDC (Grant No. IADL20210402), the National Natural Science Foundation of China (Grant Nos. 12002350, 12172314, 11772278 and 11904300), the Jiangxi Provincial Outstanding Young Talents Program (Grant No. 20192BCBL23029), the Fundamental Research Funds for the Central Universities (Xiamen University: Grant No. 20720210025).

Appendix A. Supplementary data

Supplementary data to this article can be found online at https://doi.org/10.1016/j.petsci.2023.08.009.

References

Aman, Z.M., Sloan, E.D., Sum, A.K., et al., 2014. Adhesion force interactions between cyclopentane hydrate and physically and chemically modified surfaces. Phys. Chem. Chem. Phys. 16 (45), 25121–25128. https://doi.org/10.1039/c4cp02927e.

Beemer, D.L., Wang, W., Kota, A.K., 2016. Durable gels with ultra-low adhesion to ice. J. Mater. Chem. A 4 (47), 18253–18258. https://doi.org/10.1039/c6ta07262c.

Charlton, T.B., Di Lorenzo, M., Zerpa, L.E., et al., 2018. Simulating hydrate growth and transport behavior in gas-dominant flow. Energy Fuel. 32 (2), 1012–1023. https://doi.org/10.1021/acs.energyfuels.7b02199.

Dou, R., Chen, J., Zhang, Y., et al., 2014. Anti-icing coating with an aqueous lubricating layer. ACS Appl. Mater. Interfaces 6 (10), 6998–7003. https://doi.org/10.1021/am501252u.

Fan, S.S., Zhang, H., Yang, G., et al., 2020. Reduction clathrate hydrates growth rates and adhesion forces on surfaces of inorganic or polymer coatings. Energy Fuel. 34 (11), 13566–13579. https://doi.org/10.1021/acs.energyfuels.0c01904.

Fang, B., Ning, F., Ou, W., et al., 2019. The dynamic behavior of gas hydrate dissociation by heating in tight sandy reservoirs: a molecular dynamics simulation study. Fuel 258, 116106. https://doi.org/10.1016/j.fuel.2019.116106.

Golovin, K., Kobaku, S.P.R., Lee, D.H., et al., 2016. Designing durable icephobic surfaces. Sci. Adv. 2 (3), 1501496. https://doi.org/10.1126/sciadv.1501496.

Hu, P., Wu, G.Z., Zi, M.C., et al., 2019. Effects of modified metal surface on the formation of methane hydrate. Fuel 257, 115720. https://doi.org/10.1016/j.fuel.2019.116452.

Ibanez-Ibanez, P.F., Ruiz-Cabello, F.J.M., Cabrerizo-Vilchez, M.A., et al., 2022. Ice adhesion of PDMS surfaces with balanced elastic and water-repellent properties. J. Colloid Interface Sci. 608, 792–799. https://doi.org/10.1016/j.jcis.2021.10.005.

Kendall, K., 1971. The adhesion and surface energy of elastic solids. J. Phys. D Appl. Phys. 4 (8), 1186. https://doi.org/10.1088/0022-3727/4/8/320.

Kim, J., Chisholm, B.J., Bahr, J., 2007. Adhesion study of silicone coatings: the interaction of thickness, modulus and shear rate on adhesion force. Biofouling 23 (2), 113–120. https://doi.org/10.1080/08927010701189708.

Li, T., Zhuo, Y.Z., Hakonsen, V., et al., 2019. Durable low ice adhesion foams modulated by submicrometer pores. Ind. Eng. Chem. Res. 58 (38), 17776–17783. https://doi.org/10.1021/acs.iecr.9b02939.

Li, T., Ibanez-Ibanez, P.F., Hakonsen, V., et al., 2020. Self-deicing electrolyte hydrogel surfaces with Pa-level ice adhesion and durable antifreezing/antifrost performance. ACS Appl. Mater. Interfaces 12 (31), 35572–35578. https://doi.org/10.1021/acsami.0c06912.

Li, T., Xu, K., Shi, L.X., et al., 2022. Dual-ionic hydrogels with ultralong antidehydration lifespan and superior anti-icing performance. Appl. Mater. Today 26, 101367. https://doi.org/10.1016/j.apmt.2022.101367.

Li, Y.C., Luo, C.H., Li, X.H., et al., 2016. Submicron/nano-structured icephobic surfaces made from fluorinated polymethylsiloxane and octavinyl-POSS. Appl. Surf. Sci. 360, 113–120. https://doi.org/10.1016/j.apsusc.2015.10.193.

Lin, Y., Li, T., Liu, S., et al., 2022a. Interfacial mechanical properties of tetrahydrofuran hydrate-solid surfaces: implications for hydrate management. J. Colloid Interface Sci. 629, 326–335. https://doi.org/10.1016/j.jcis.2022.09.081.

Lin, Y., Liu, Y., Xu, K., et al., 2022b. Strengthening and weakening of methane hydrate by water vacancies. Adv. Geo-Energy Res. 6 (1), 23–37. https://doi.org/10.46690/ager.2022.01.03.

Liu, C.W., Wang, Z.Y., Tian, J.L., et al., 2020a. Fundamental investigation of the adhesion strength between cyclopentane hydrate deposition and solid surface materials. Chem. Eng. Sci. 217. https://doi.org/10.1016/j.ces.2020.115524.

Liu, C.W., Zeng, X., Yan, C., et al., 2020b. Effects of solid precipitation and surface corrosion on the adhesion strengths of sintered hydrate deposits on pipe walls. Langmuir 36 (50), 15343–15351. https://doi.org/10.1021/acs.langmuir.0c02818.

Liu, C.W., Liang, Y., Chenru, Z., et al., 2022. Effects of hydrate inhibitors on the adhesion strengths of sintered hydrate deposits on pipe walls. J. Colloid Interface Sci. 624, 593–601. https://doi.org/10.1016/j.jcis.2022.06.004.

Ma, R., Wang, F., Chang, Y.H., et al., 2021. Unraveling adhesion strength between gas hydrate and solid surfaces. Langmuir 37 (47), 13873–13881. https://doi.org/10.1021/acs.langmuir.1c02315.

Nahri, S.Y., Nielsen, J.L., Chen, Y., 2019. Effect of nanoparticles on the nucleation and agglomeration rates of hydrate growth using THF-water clathrates. Petrol. Sci. 17 (2), 467–476. https://doi.org/10.1007/s12182-019-00390-4.

Ning, F.L., Yu, Y.B., Kjelstrup, S., et al., 2012. Mechanical properties of clathrate hydrates: status and perspectives. Energy Environ. Sci. 5 (5), 6779–6795. https://doi.org/10.1039/c2ee03435b.

Pang, X.Q., Chen, Z.H., Jia, C.Z., et al., 2021. Evaluation and re-understanding of the global natural gas hydrate resources. Petrol. Sci. 18 (2), 323–338. https://doi.org/10.1007/s12182-021-00568-9.

Ragunathan, T., Xu, X.G., Shuhili, J.A., et al., 2019. Preventing hydrate adhesion with magnetic slippery surfaces. ACS Omega 4 (14), 15789–15797. https://doi.org/10.1021/acsomega.9b01232.

Regulagadda, K., Gerber, J., Schutzius, T.M., et al., 2022. Microscale investigation on interfacial slippage and detachment of ice from soft materials. Mater. Horiz. 9 (4), 1222–1231. https://doi.org/10.1039/d1mh01993g.

Sloan, E.D., 2003. Fundamental principles and applications of natural gas hydrates. Nature 426 (6964), 353–359. https://doi.org/10.1038/nature02135.

Smith, J.D., Meuler, A.J., Bralower, H.L., et al., 2012. Hydrate-phobic surfaces: fundamental studies in clathrate hydrate adhesion reduction. Phys. Chem. Chem. Phys. 14 (17), 6013–6020. https://doi.org/10.1039/c2cp40581d.

Sojoudi, H., Walsh, M.R., Gleason, K.K., et al., 2015. Investigation into the formation and adhesion of cyclopentane hydrates on mechanically robust vapor-deposited polymeric coatings. Langmuir 31 (22), 6186–6196. https://doi.org/10.1021/acs.langmuir.5b00413.

Sojoudi, H., Arabnejad, H., Raiyan, A., et al., 2018. Scalable and durable polymeric icephobic and hydrate-phobic coatings. Soft Matter 14 (18), 3443–3454. https://doi.org/10.1039/c8sm00225h.

Sum, A.K., Koh, C.A., Sloan, E.D., 2009. Clathrate hydrates: from laboratory science to engineering practice. Ind. Eng. Chem. Res. 48 (16), 7457–7465. https://doi.org/10.1021/ie900679m.

Wang, C.Y., Fuller, T., Zhang, W., et al., 2014. Thickness dependence of ice removal stress for a polydimethylsiloxane nanocomposite: Sylgard 184. Langmuir 30 (43), 12819–12826. https://doi.org/10.1021/la5030444.

Wang, F., Ma, R., Xiao, S.B., et al., 2022a. Anti-gas hydrate surfaces: perspectives, progress and prospects. J. Mater. Chem. A 10 (2), 379–406. https://doi.org/10.1039/d1ta08965j.

Wang, P., Wang, J., Xu, K., et al., 2022b. Mechanical stability of fluorinated-methane clathrate hydrates. J. Mol. Liq. 360, 119553. https://doi.org/10.1016/j.molliq.2022.119553.

Wang, Y.H., Fan, S.S., Lang, X.M., 2019. Reviews of gas hydrate inhibitors in gas-dominant pipelines and application of kinetic hydrate inhibitors in China. Chin. J. Chem. Eng. 27 (9), 2118–2132. https://doi.org/10.1016/j.cjche.2019.02.023.

Wu, J.Y., Ning, F.L., Trinh, T.T., et al., 2015. Mechanical instability of monocrystalline and polycrystalline methane hydrates. Nat. Commun. 6 (1), 8743. https://doi.org/10.1038/ncomms9743.

Wu, J.Y., Skallerud, B., He, J.Y., et al., 2017. Grain-size induced strengthening and weakening of dislocation-free polycrystalline gas hydrates. 2016 Iutam Symp.Nanos.Phys.Mech. 21, 11–16. https://doi.org/10.1016/j.piutam.2017.03.031.

Xu, K., Yang, L., Liu, J., et al., 2020. Mechanical properties of CH_4-CO_2 heteroclathrate hydrates. Energy Fuel. 34 (11), 14368–14378. https://doi.org/10.1021/acs.energyfuels.0c02430.

Xu, K., Lin, Y., Li, T., et al., 2022a. Structural and mechanical stability of clathrate hydrates encapsulating monoatomic guest species. J. Mol. Liq. 347, 118391. https://doi.org/10.1016/j.molliq.2021.118391.

Xu, K., Lin, Y., Shi, Q., et al., 2022b. Role of mechanical deformation in the thermal transport of sI-type methane hydrate. Phys. Chem. Chem. Phys. 24 (9), 5479–5488. https://doi.org/10.1039/d1cp04189d.

Yang, L., Guan, D., Qu, A., et al., 2023. Thermotactic habit of gas hydrate growth enables a fast transformation of melting ice. Appl. Energy 331, 120372. https://doi.org/10.1016/j.apenergy.2022.120372.

Yeong, Y.H., Wang, C.Y., Wynne, K.J., et al., 2016. Oil-infused superhydrophobic silicone material for low ice adhesion with long-term infusion stability. ACS Appl. Mater. Interfaces 8 (46), 32050–32059. https://doi.org/10.1021/acsami.6b11184.

Yeong, Y.H., Milionis, A., Loth, E., et al., 2018. Self-lubricating icephobic elastomer coating (SLIC) for ultralow ice adhesion with enhanced durability. Cold Reg. Sci. Technol. 148, 29–37. https://doi.org/10.1016/j.coldregions.2018.01.005.

Zhang, H., Du, J.W., Wang, Y.H., et al., 2018. Investigation into THF hydrate slurry flow behaviour and inhibition by an anti-agglomerant. RSC Adv. 8 (22), 11946–11956. https://doi.org/10.1039/c8ra00857d.

Zhang, W.J., Fan, S.S., Wang, Y.H., et al., 2021. Preparation and performance of biomimetic superhydrophobic coating on X80 pipeline steel for inhibition of hydrate adhesion. Chem. Eng. J. 419, 129651. https://doi.org/10.1016/j.cej.2021.129651.

Zhang, X.W., Straume, E.O., Grasso, G.A., et al., 2020. A bench-scale flow loop study on hydrate deposition under multiphase flow conditions. Fuel 262, 116558. https://doi.org/10.1016/j.fuel.2019.116558.